Supporting information

Highly Active and Stable Metal Single-Atom Catalysts Achieved by Strong Electronic Metal-Support Interactions

Junjie Li,[†, ‡, ⊥] Qiaoqiao Guan,[†, ‡, ⊥] Hong Wu,[¶, ⊥] Wei Liu,[§] Yue Lin,[†] Zhihu Sun,[§] Xuxu Ye,[¶] Xusheng Zheng,[§] Haibin Pan,[§] Junfa Zhu,[§] Si Chen,[¶] Wenhua Zhang,[†, ¶, ǁ] Shiqiang Wei,[§] Junling Lu,[†, ‡, ¶, *]

[†]Hefei National Laboratory for Physical Sciences at the Microscale, University of Science and Technology of China, Hefei, Anhui 230026 China
[‡]Department of Chemical Physics, *i*Chem, University of Science and Technology of China, Hefei, Anhui 230026 China
[¶]CAS Key Laboratory of Materials for Energy Conversion, University of Science and Technology of China, Hefei, Anhui 230026 China
[§]National Synchrotron Radiation Laboratory, University of Science and Technology of China, Hefei, Anhui 230029 China
[ǁ]Synergetic Innovation Centre of Quantum Information & Quantum Physics, University of Science and Technology of China, Hefei, Anhui 230026 China

*To whom correspondence should be addressed. E-mail: junling@ustc.edu.cn

Experimental section

1. Catalyst synthesis

Support materials. Co_3O_4 (metals basis, 99%) and ZrO_2 (metals basis, 99%) were purchased from Alfa Aesar and used without further treatments. The graphene support was prepared through the thermal reduction of graphene oxide. The detailed procedure can be found in our previous work.[1]

CeO_2 nanorods were synthesized by the template-free hydrothermal method.[2] Typically, 1.73 g $Ce(NO_3)_3 \cdot 6H_2O$ (Sinopharm Chemical Reagent Co., Ltd AR grade) and 19.2 g NaOH (Sinopharm Chemical Reagent Co., Ltd AR grade) were dissolved in 10 and 70 mL ultrapure water, respectively. Next, the $Ce(NO_3)_3$ and NaOH solutions were transferred to a constant pressure drop funnel and three neck flask, respectively. Ar gas (99.999%, Nanjing Special Gases) was introduced for a few minutes to replace the air. Next, the $Ce(NO_3)_3$ solution was added to the NaOH solution rapidly with stirring to get a milk white slurry. The slurry was transferred to a 100 mL Teflon bottle quickly to perform the hydrothermal treatment at 100 °C for 24 h. Next, fresh white precipitates were separated by centrifugation, and washed by ultrapure water 5 times. The resulting materials was further dried at 60 °C in air overnight to the CeO_2 nanorods.

Synthesis of Pt_1/Co_3O_4, Pt_1/CeO_2, Pt_1/ZrO_2 and Pt_1/graphene single-atom catalysts. Pt ALD was carried out on a viscous flow reactor (GEMSTAR-6™ Benchtop ALD, Arradiance) by exposing to trimethyl (methylcyclopentadienyl)-platinum (IV) ($MeCpPtMe_3$, Sigma-Aldrich, 98%) at 80, 150, 120 and 250 °C for Pt_1/Co_3O_4, Pt_1/CeO_2, Pt_1/ZrO_2 and Pt_1/graphene, respectively. Ultrahigh purity N_2 (99.999%, Nanjing Special Gases) was used as a carrier gas at a flow rate of 200 mL/min. The Pt precursor was heated to 65 °C to get sufficient vapor pressure and the reactor inlets were heated to 80 °C to avoid any condensation. The support was loaded into the ALD reactor. After temperature stabilization, one cycle of Pt ALD was conducted to prepare the Pt SACs. Here ozone was used to burn off the $MeCpPtMe_3$ precursor ligand for synthesis of Pt_1/Co_3O_4, Pt_1/CeO_2, and Pt_1/ZrO_2 SACs. While oxygen was used as the oxidant for synthesis of Pt_1/graphene. The timing sequence was 200, 250, 100, and 150 sec for the

$MeCpPtMe_3$ exposure, N_2 purge, O_2 (or O_3) exposure, and N_2 purge, respectively.

Synthesis of Pt-NPs/Co_3O_4. To obtain Pt NPs on the Co_3O_4 support, Pt ALD was carried out at 300 °C for two cycles by alternatively exposing to $MeCpPtMe_3$ and O_2. The timing sequence was 200, 250, 100, and 150 sec for the $MeCpPtMe_3$ exposure, N_2 purge, O_2 exposure, and N_2 purge, respectively.

Synthesis of Pt/SiO_2 and Pt/Al_2O_3. Pt/SiO_2 and Pt/Al_2O_3 were also synthesized through a wet-impregnation method for a comparison.[3] Typically, 100 mg SiO_2 or Al_2O_3 support was slowly added into a 1.9×10^{-2} M H_2PtCl_6 aqueous solution (0.9 mL). Then, the mixture was stirred for 30 min, and dried in air at room temperature for 12 h. The dried material was first calcined in air at 120 °C for 12 h, and then reduced in 10% H_2 in argon at 300 °C for another 2 h at a flow rate of 60 mL/min to get the Pt/SiO_2 and Pt/Al_2O_3 samples.

Synthesis of Pd_1/Co_3O_4 and Pd-NPs/Co_3O_4.

Pd ALD was performed at 200 °C, using palladium hexafluoroacetylacetate ($Pd(hfac)_2$, (Sigma-Aldrich, 99.9%) and formalin (Aldrich, 37% HCHO and 15% CH_3OH in aqueous solution).[4] The Pd precursor and the inlets were heated to 65 and 115 °C. The Pd_1/Co_3O_4 was synthesized by performing one cycle of Pd ALD. The timing sequence was 180, 200, 60 and 200 sec for $Pd(hfac)_2$ exposure, N_2 purge, formalin exposure and N_2 purge, respectively. The Pd nanoparticle sample of Pd-NPs/Co_3O_4 was synthesized by using the same time sequence for four cycles.

2. Catalyst characterization

The Pt or Pd loadings on catalysts were determined by an inductively coupled plasma atomic emission spectrometer (ICP-AES). All samples were dissolved in hot fresh aqua regia for ICP-AES testing.

The morphology of catalysts was characterized on an aberration-corrected HAADF-STEM instrument at 200 kV (JEOL-2010F, University of Science and Technology of China) and transmission electron microscopy (TEM, JEOL-2010) at 200 kV.

X-ray photoelectron spectroscopy (XPS) measurements were taken on a Thermo-VG Scientific Escalab 250 spectrometer, equipped with an aluminum anode (Al Kα = 1486.6 eV) (Hefei University of Technology).

Diffuse reflectance infrared Fourier transform spectroscopy (DRIFTS) CO chemisorption measurements were performed on a Nicolet iS10 spectrometer equipped with an MCT detector and a low temperature reaction cell (Praying Mantis Harrick). The sample was first pretreated in 10% O_2 in Ar at 150 °C to remove any contaminant. After cooling the sample to room temperature under Ar, a background spectrum was collected. Then the sample was exposed to 10% CO in Ar at a flow rate of 20 mL/min for about 30 min until saturation. Next, Ar (99.999%) was introduced at a flow rate of 20mL/min for another 30 min to remove the gas phase CO and then the DRIFT spectrum was collected with 256 scans at a resolution of 4 cm^{-1}.

X-ray absorption spectroscopy (XAS) measurements at the Pt L_3-edge (11564 eV) were performed in the transmission mode with the Si (111) monochromator at the BL14W1 beamline of the Shanghai Synchrotron Radiation Facility (SSRF), China. The storage ring of SSRF worked at 3.5 GeV with a maximum current of 210 mA.

Hydrogen temperature-programmed reduction (H_2 -TPR) was performed on a Micromeritics Autochem II 2920 instrument. Each sample was first pretreated in 10% O_2 in Ar at 200 °C for 60 min. Next, the sample was cooled to 0 °C in Ar and wait for 30 min until the baseline became stable. TPR was performed by heating the sample at 10 °C/min up to 550 °C in 10% H_2 in Ar and a cooled trap with an isopropyl alcohol/liquid nitrogen slurry at -80 ˚C was used before the TCD detector to retain the produced water.

3. Catalytic testing

Hydrolytic dehydrogenation of ammonia borane was conducted in a home-made gas generation setup, which can be found elsewhere.[5] The hydrolytic dehydrogenation of ammonia borane (AB, Aldrich 97%) was kept in a three-necked round bottom flask at 25 °C under atmospheric pressure. 10 mg of the Pt_1/Co_3O_4 or Pd_1/Co_3O_4 catalyst was used, while the weight of other catalysts was adjusted to keep the same amount of metal

content. Typically, 5 mL aqueous AB solution (6.5×10^{-2} M) was introduced into the glass container via a syringe. The AB solution and the catalyst were well-mixed by using a magnetic stirrer and vigorously stirred with a magnetic stirrer during the reaction. The generated volume of H_2 was measured by a water-filled gas burette.

The specific rates (r) of these catalysts were calculated according to the Eq. (1):

$$r = \frac{n_{gas}}{n_{metal}} \cdot \frac{1}{t} \quad (1)$$

Here n_{gas} is the mole of generated H_2, while n_{metal} is the total mole of Pt or Pd in the sample. t is the reaction time in min.

According to the durability test, another equivalent amount of AB was added into the three-necked flask after the hydrogen generation reaction was completed. Then the generated volume of H_2 by the water-filled gas burette with reaction time was recorded. Similar operations were repeated for 15 times.

For kinetic studies, the hydrolytic dehydrogenation of AB reaction was also carried out at 30, 35 and 40 °C, in order to obtain the activation energy (E_a).

Selective hydrogenation of 1,3-butadiene was performed in a fixed-bed quartz tube reactor at an atmospheric pressure. The feed gas consists of 2.0 % 1,3 butadiene, 4.0 % H_2 with Ar as balance gas. The total flow rate was kept at 25 mL/min. 75 mg Pt_1/Co_3O_4 catalyst was used, while the amount of other catalysts was adjusted to keep the same Pt content. All catalysts were diluted with 1 g of 60-80 mesh quartz chips. Prior to the reaction test, all catalysts were first calcined in 10% O_2 in Ar for 1 h. The reaction products were analyzed using an online gas chromatography equipped with a flame ionization detector and a capillary column (ValcoPLOT VP-Alumina, 50 m x 0.53 mm) after stabilizing in the feed gas for 2 h. Next, the 1,3-butadiene conversion on all these catalysts was increased by increasing the reaction temperatures.

4. DFT calculations

All the calculations were performed by spin-polarized density functional theory (DFT) as implemented in the Vienna ab initio simulation package (VASP).[6] The exchange–correlation interaction is described by the generalized gradient

approximation (GGA) with the Perdew–Burke–Ernzerhof (PBE) functional.[7] A kinetic cutoff energy of 400 eV was applied for plane wave expansions. The convergence criteria for the total energy and the forces were set as 10^{-5} eV and 0.02 eV $Å^{-1}$, respectively. DFT+U corrections[8] with U_{eff} =3.5, 5.0 and 4.0 eV[9] were applied for Co 3*d*-orbitals, Ce 4*f*-orbitals and Zr 3*d*-orbitals, respectively.

The adsorption energy is calculated by the formula: $E_{ad} = E_{(adsorbate/catalyst)} - (E_{catalyst} + E_{adsorbate})$, where $E_{(adsorbate/catalyst)}$, $E_{catalyst}$ and $E_{adsorbate}$ are the total energies of specie AB (or H_2) adsorbed on the surface, the bare surface and the gas phase molecule AB (or H_2) in its ground state, respectively. The binding energy (E_{BE}) of Pt_1 on various metal oxides are calculated as $E_{BE} = E_{Pt1/MO} - E_{Pt1} - E_{V-MO}$, where $E_{Pt1/MO}$, E_{Pt1} and E_{V-MO} are the energies of Pt_1 anchored by metal oxides, single Pt_1 atom and metal oxides with Pt_1 atom removed, respectively.

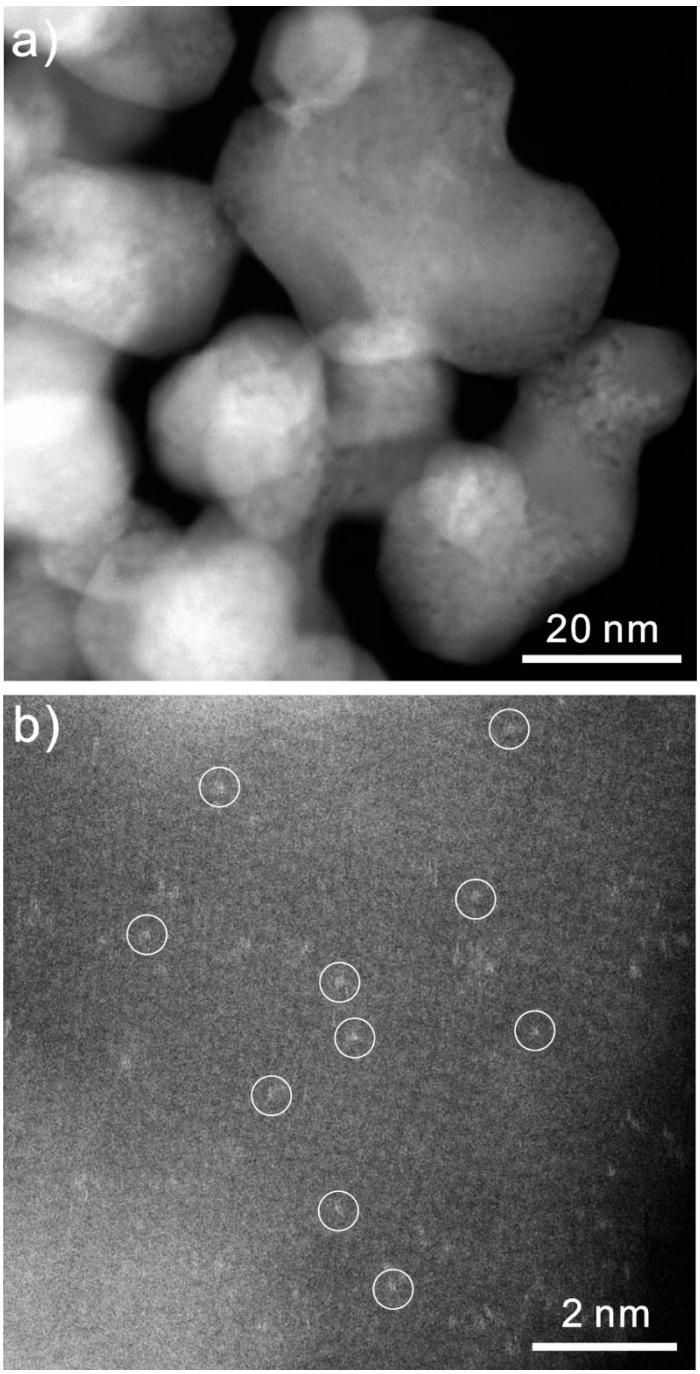

Figure S1. Representative HAADF-STEM images of Pt_1/Co_3O_4 at (a) low- and (b) high-magnifications at other locations. Representive Pt_1 single atoms in (b) are highlighted by the white circles.

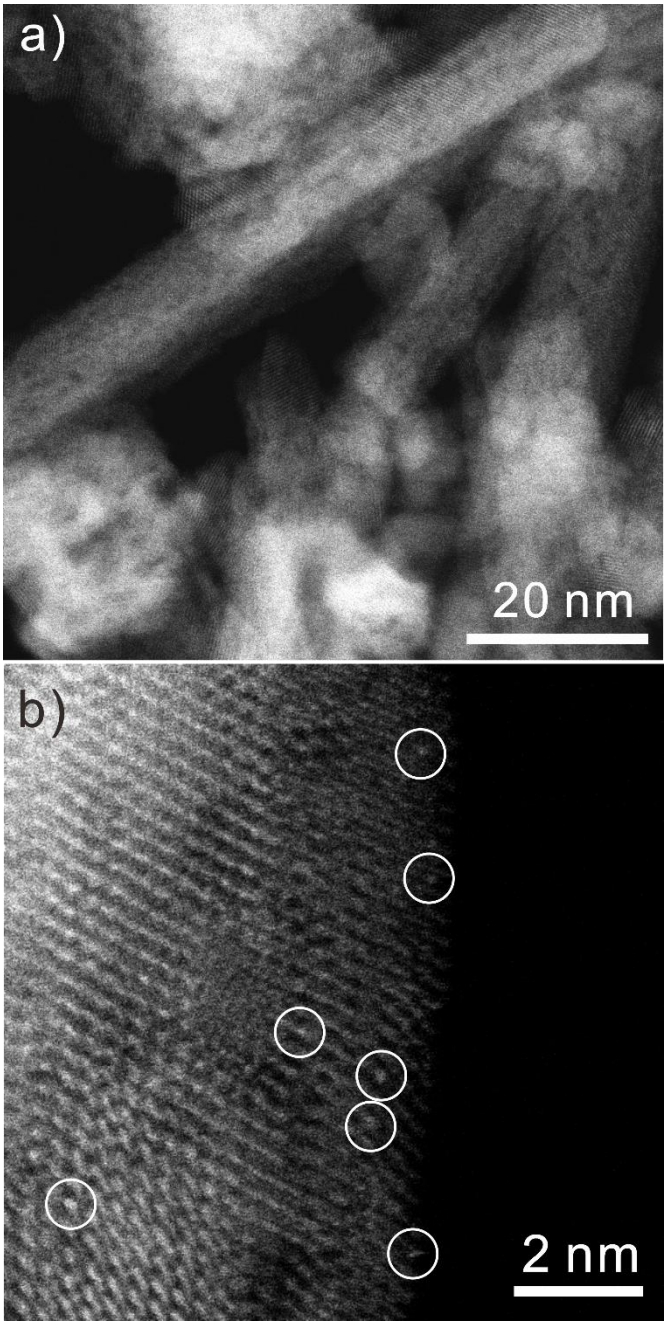

Figure S2. Representative HAADF-STEM images of Pt_1/CeO_2 at (a) low- and (b) high-magnifications at other locations. Representive Pt_1 single atoms in (b) are highlighted by the white circles.

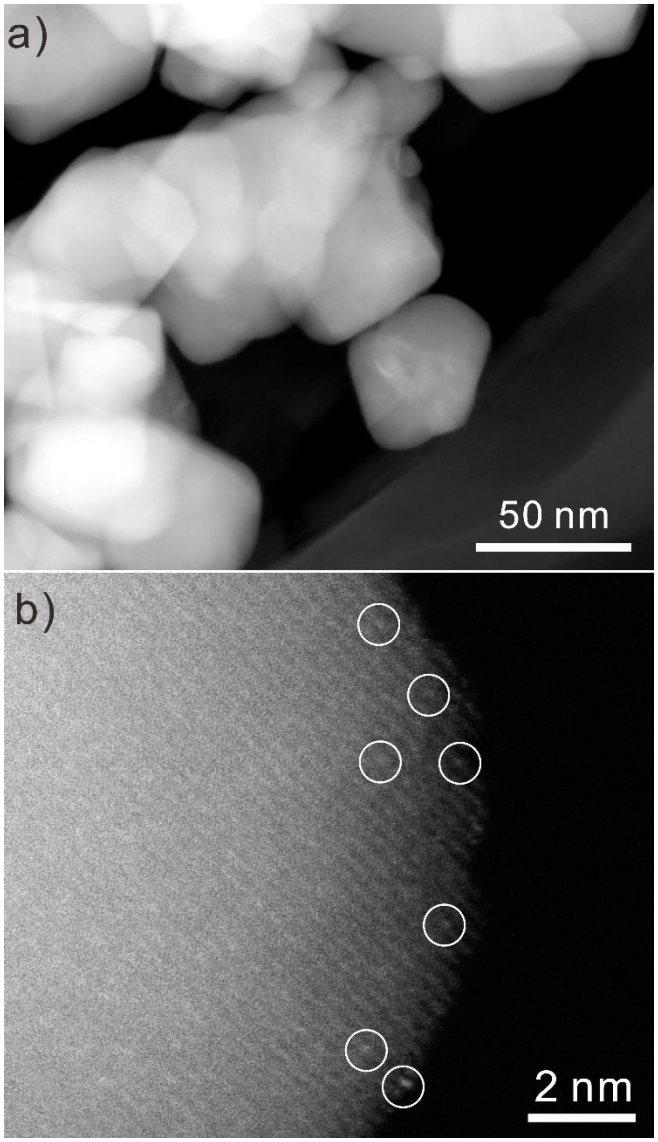

Figure S3. Representative HAADF-STEM images of Pt_1/ZrO_2 at (a) low- and (b) high-magnifications at other locations. Representive Pt_1 single atoms in (b) are highlighted by the white circles.

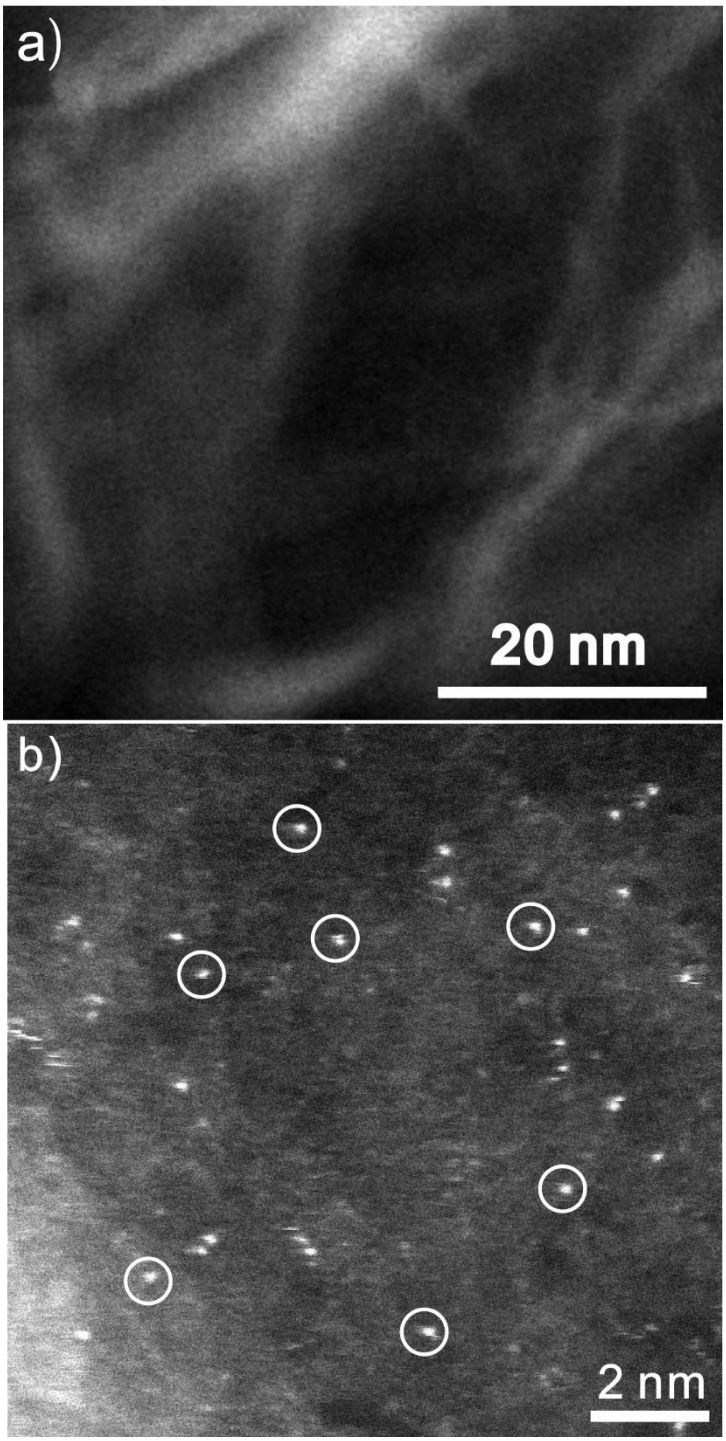

Figure S4. Representative HAADF-STEM images of Pt_1/graphene at (a) low- and (b) high-magnifications at other locations. Representive Pt_1 single atoms in (b) are highlighted by the white circles.

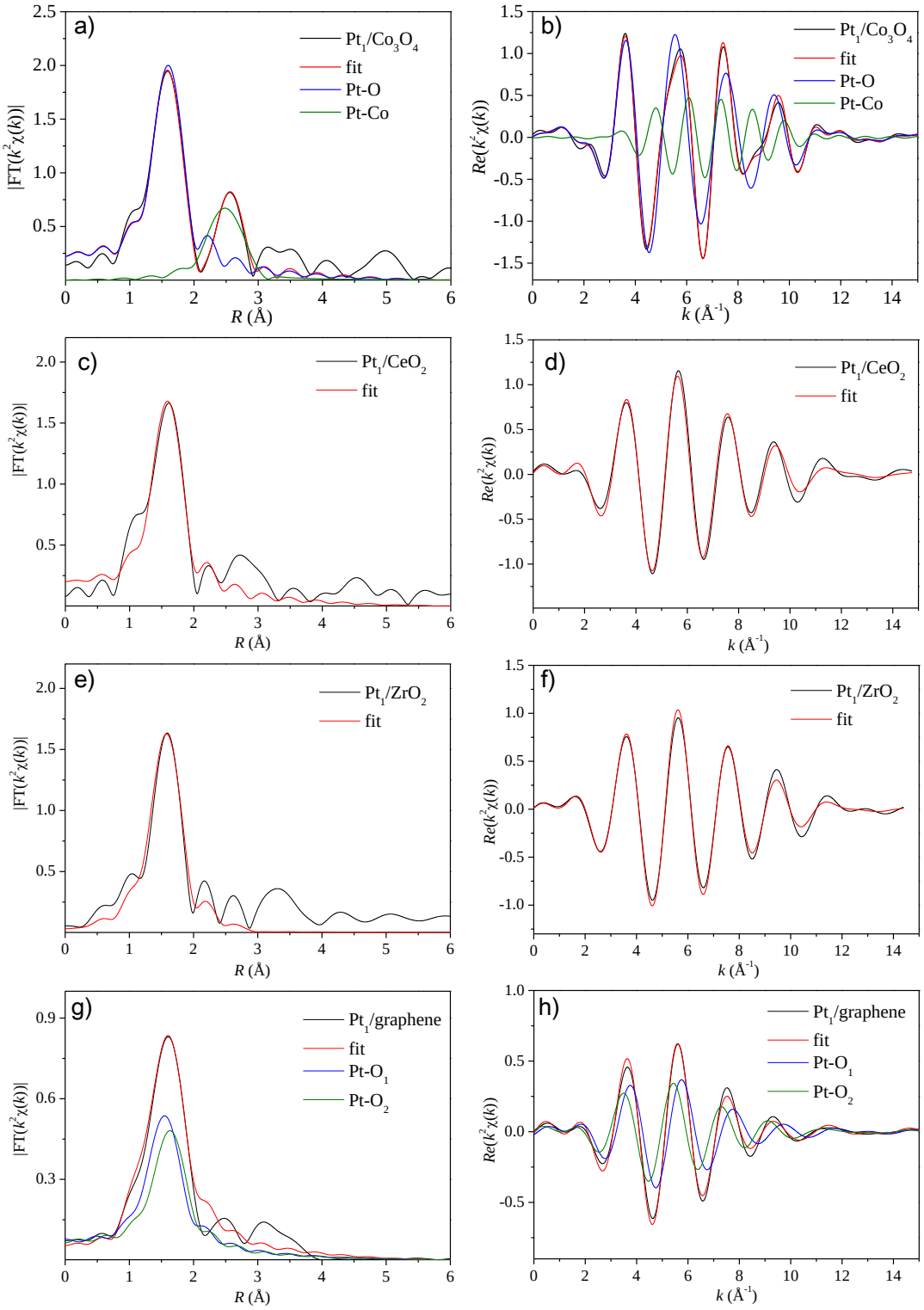

Figure S5. The Fourier transforms EXAFS fitting results of (a,b) Pt_1/Co_3O_4, (c,d) Pt_1/CeO_2, (e,f) Pt_1/ZrO_2, and (g,f) Pt_1/graphene samples at Pt L_3 edge.

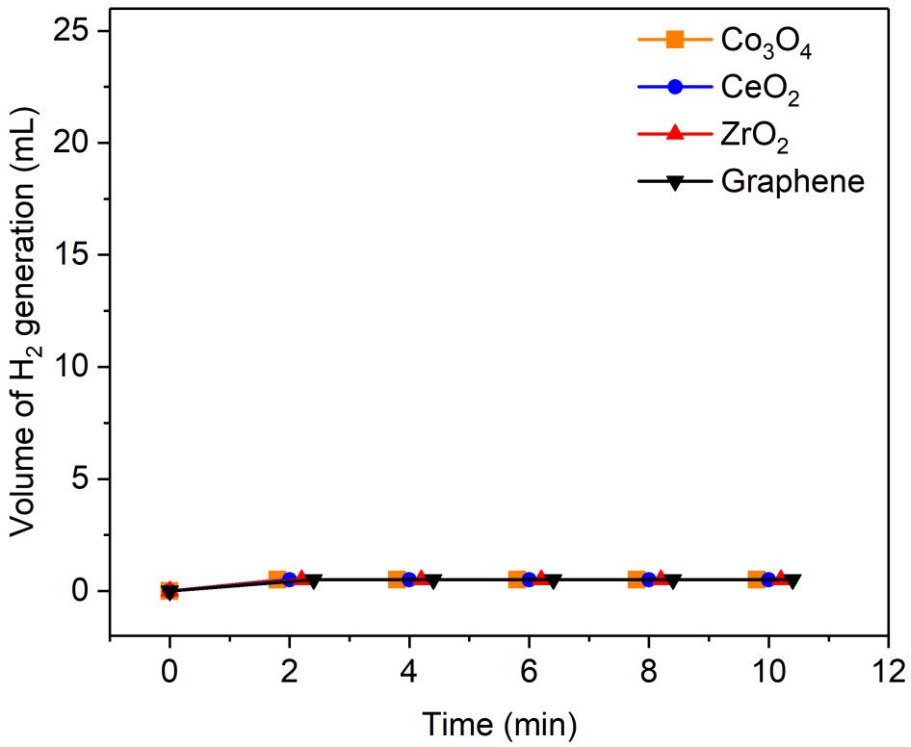

Figure S6. Plots of time vs volume of hydrogen gas generated from AB hydrolysis over four different supports.

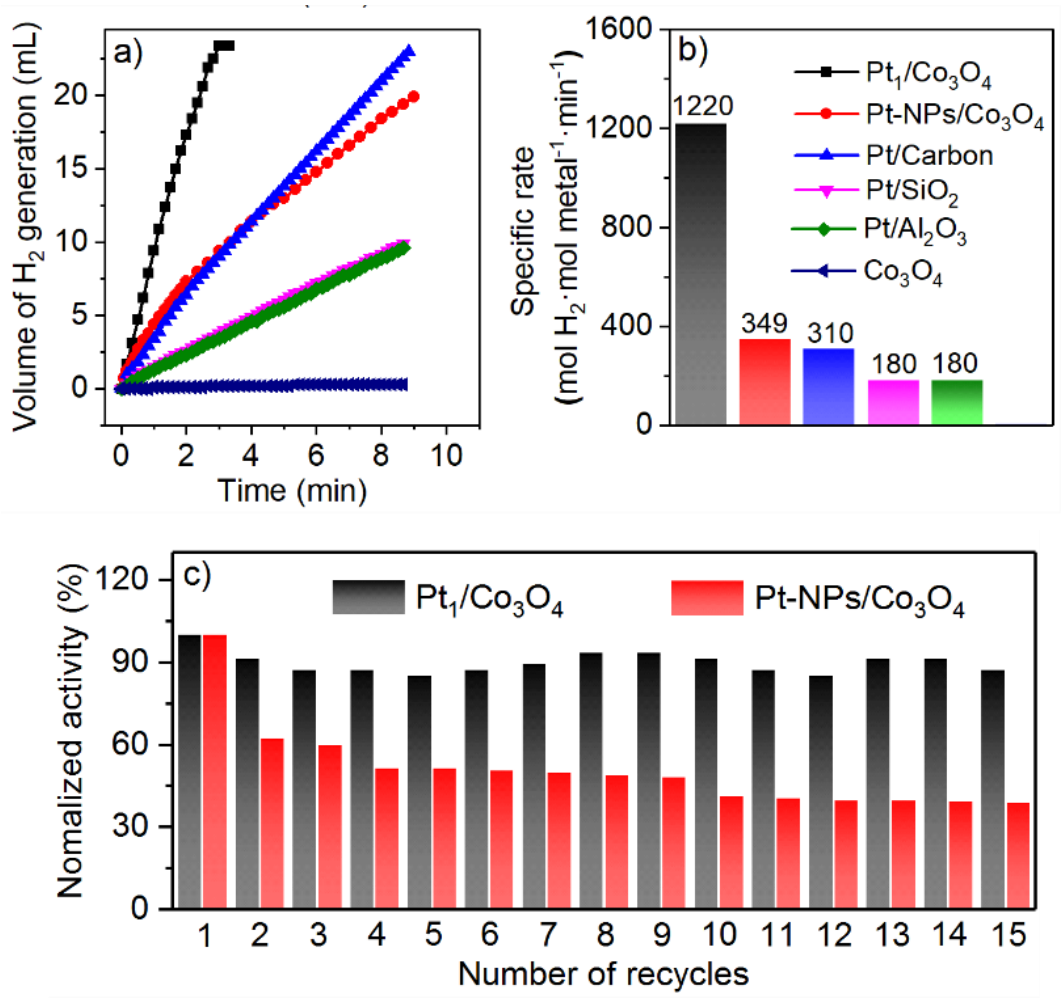

Figure S7. (a) Plots of time vs volume of hydrogen gas generated from AB hydrolysis over different Pt-based catalysts; (b) Specific rates over these samples based on the amount of Pt. (c) Durability tests on Pt_1/Co_3O_4 and Pt-NPs/Co_3O_4.

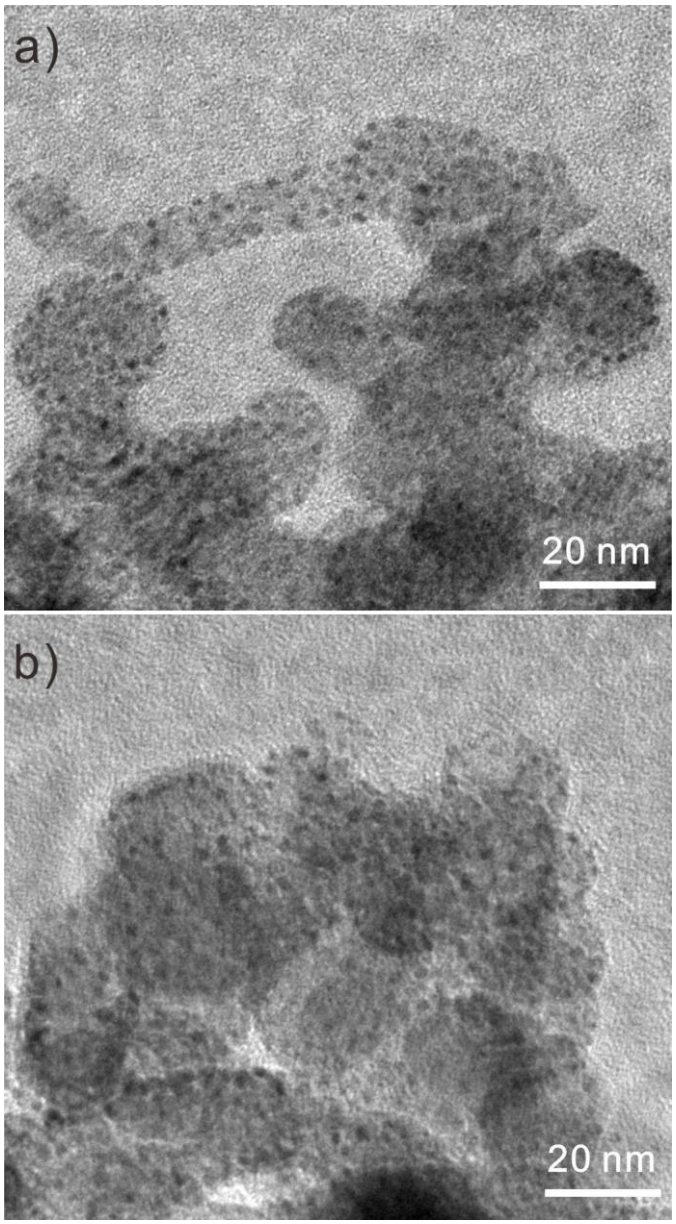

Figure S8. Representative TEM images of Pt-NPs/Co_3O_4. The average of Pt particle size was 2.3 nm

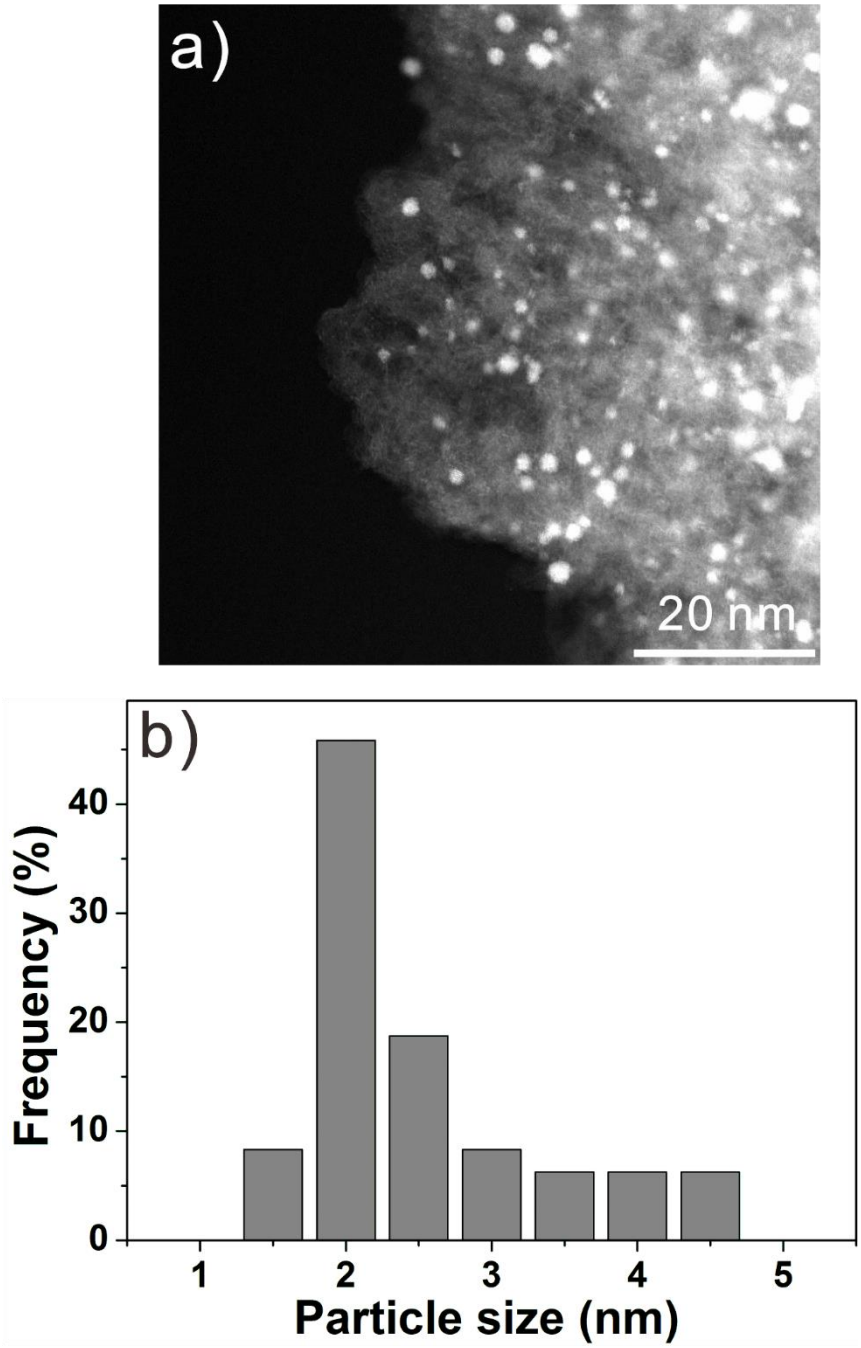

Figure S9. A representative HAADF STEM image of a commercial Pt/carbon (Sigma Aldrich) catalyst and its corresponding Pt particle distribution (b). The average of Pt particle size was 2.2 nm and the Pt loading was 5wt%.

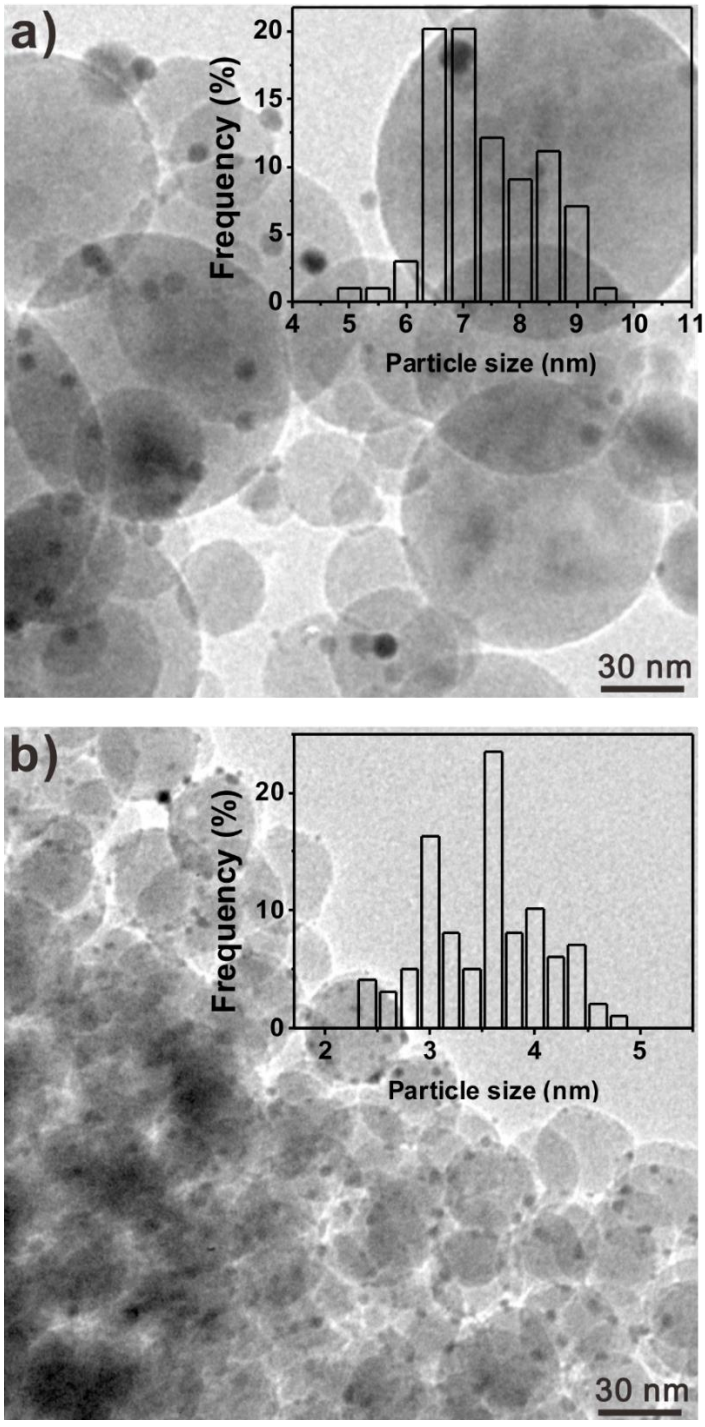

Figure S10. Representative TEM images of Pt/Al_2O_3 (a), Pt/SiO_2 (b) catalysts. The inserts showed the Pt particle size distribution. The average Pt particle size of 7.4 and 3.4 nm, and the Pt loadings of 3.7 and 3.3 wt% for Pt/Al_2O_3, Pt/SiO_2, respectively.

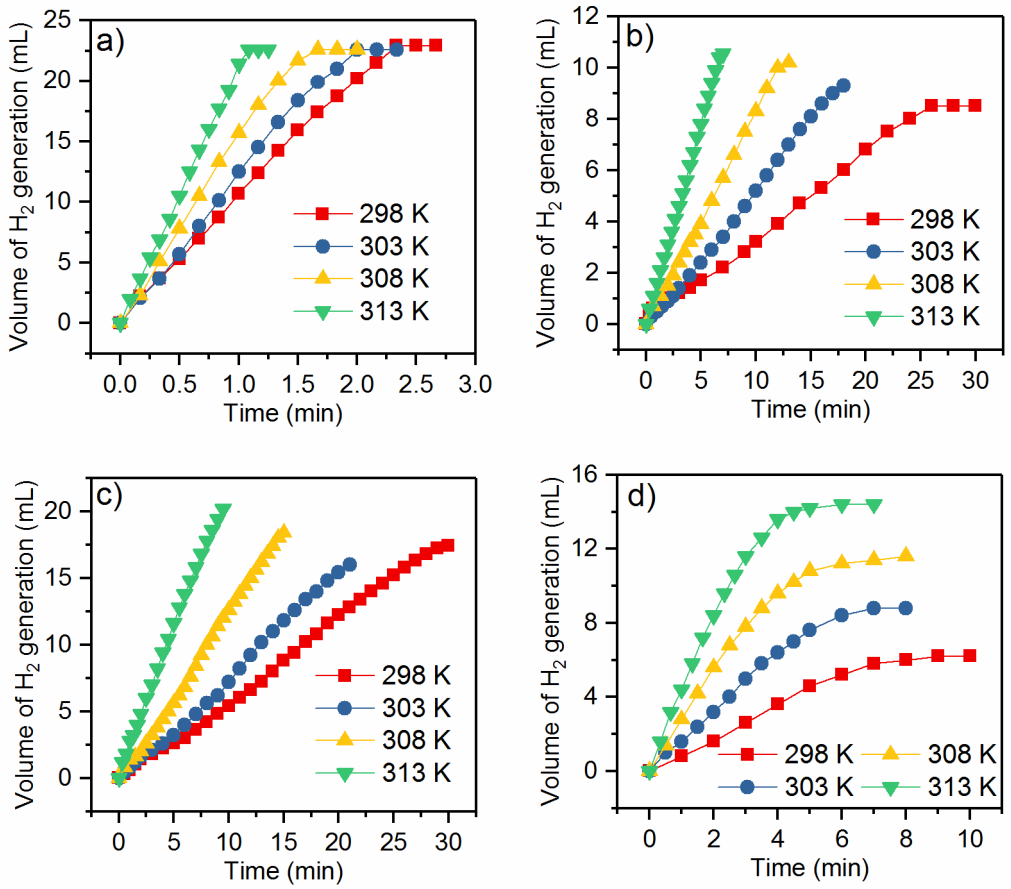

Figure S11. Temperature dependence of H_2 evolution plots from the hydrolytic dehydrogenation of AB over Pt_1/Co_3O_4 (a), Pt_1/CeO_2 (b), Pt_1/ZrO_2 (c) and Pt_1/graphene (d) SAC catalysts.

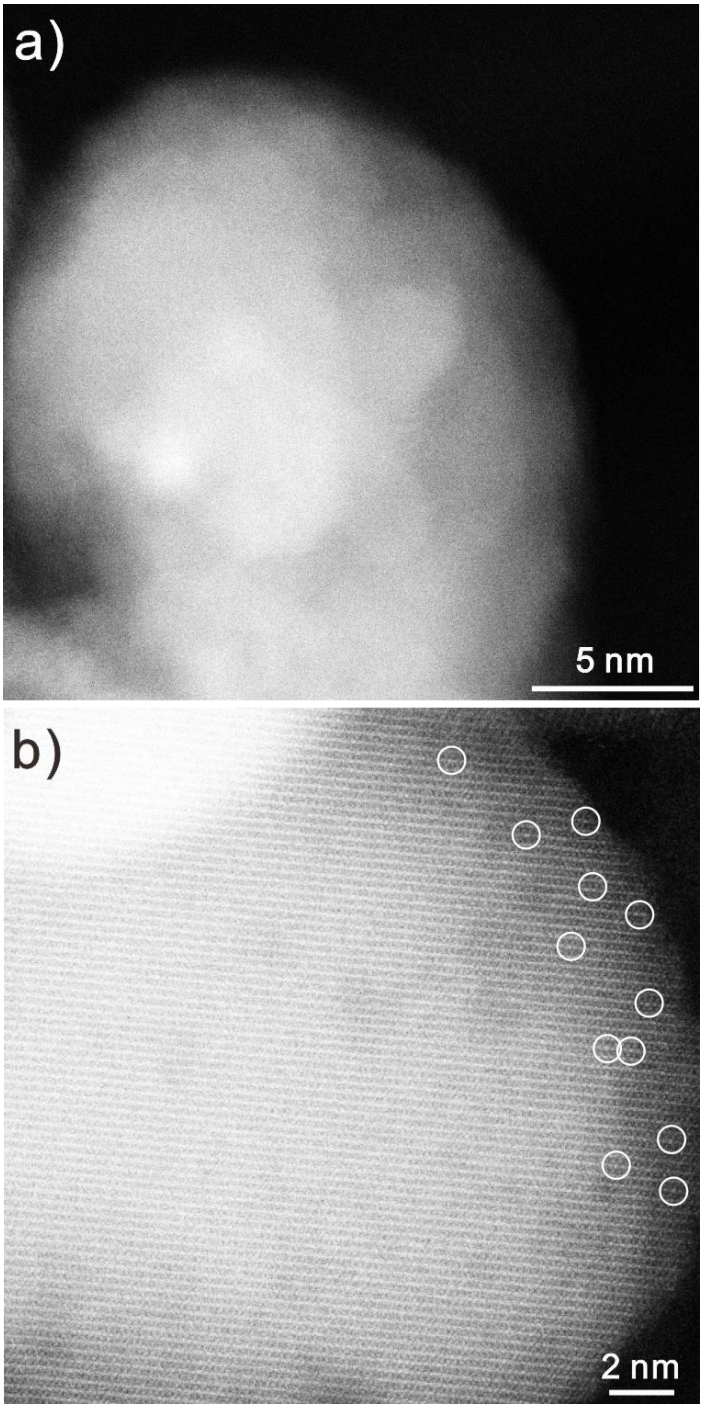

Figure S12. Representative HAADF-STEM images of Pt_1/Co_3O_4 catalysts after 15 cycles of recycling test. No obvious cluster or nanoparticle were observed. Pt_1 atoms in images are highlighted by the white circles.

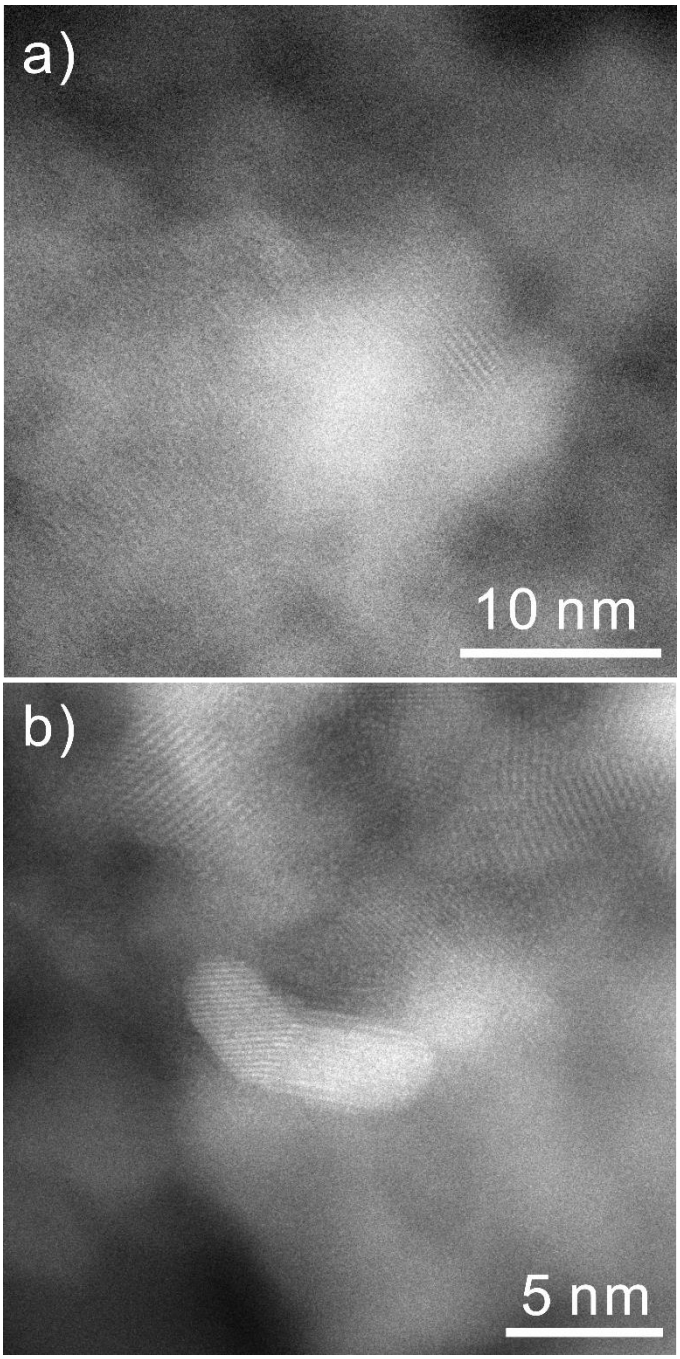

Figure S13. Representative HAADF-STEM images of Pt_1/CeO_2 catalyst after 15 cycles of recycling test. Large size of Pt nanoparticles were observed.

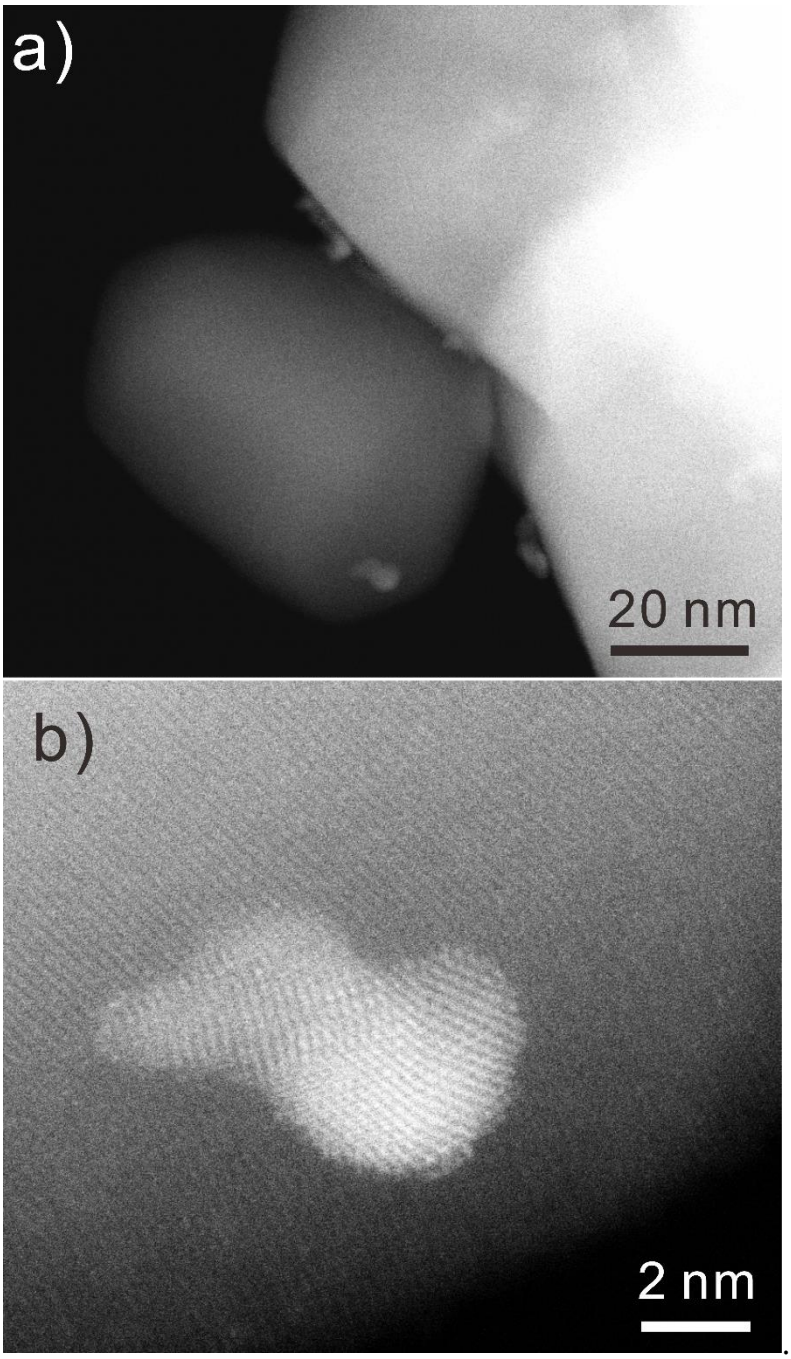

Figure S14. Representative HAADF-STEM images of Pt_1/ZrO_2 catalyst after 15 cycles of recycling test. Large size of Pt nanoparticles were observed.

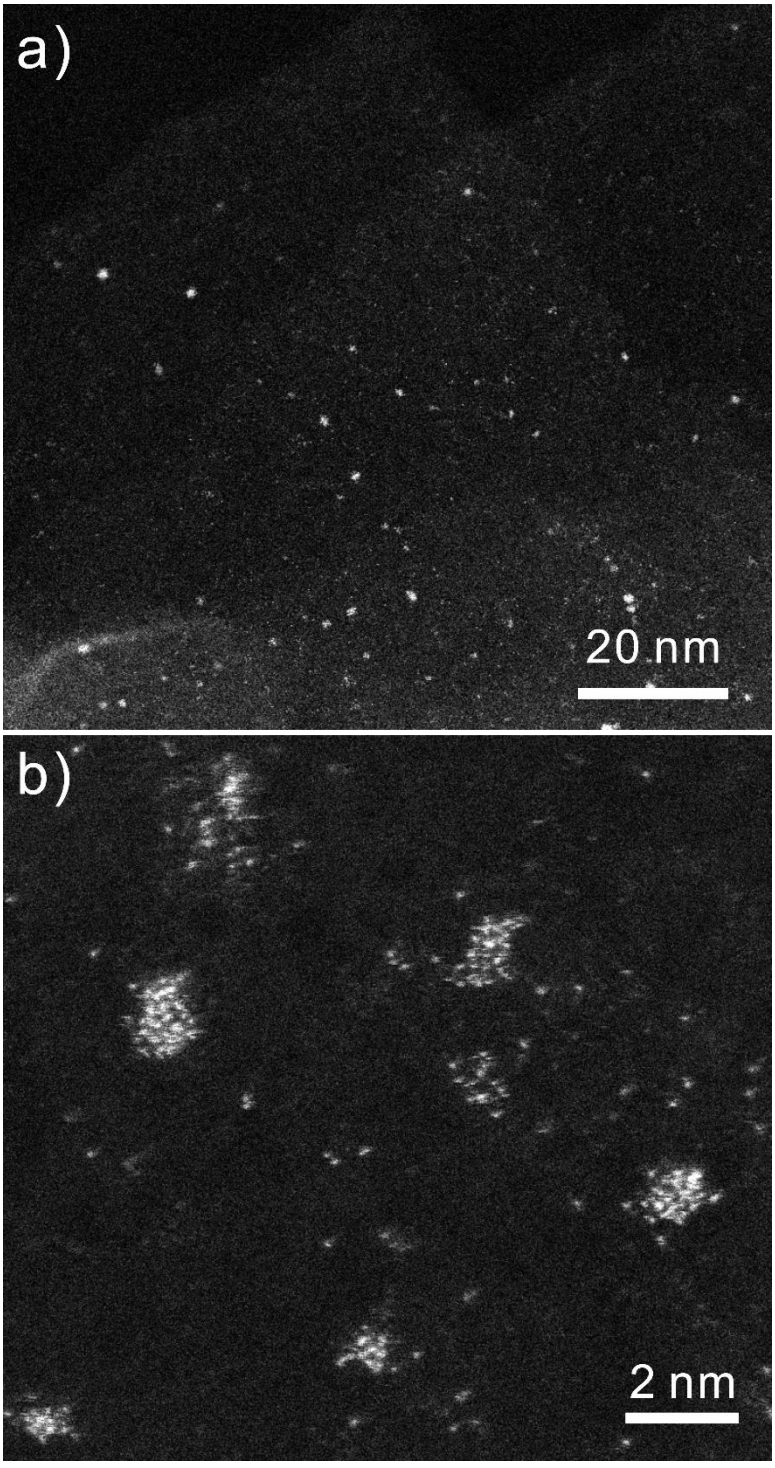

Figure S15. Representative HAADF-STEM images of Pt_1/graphene catalyst after 15 cycles of recycling test. Pt nanoparticles were observed.

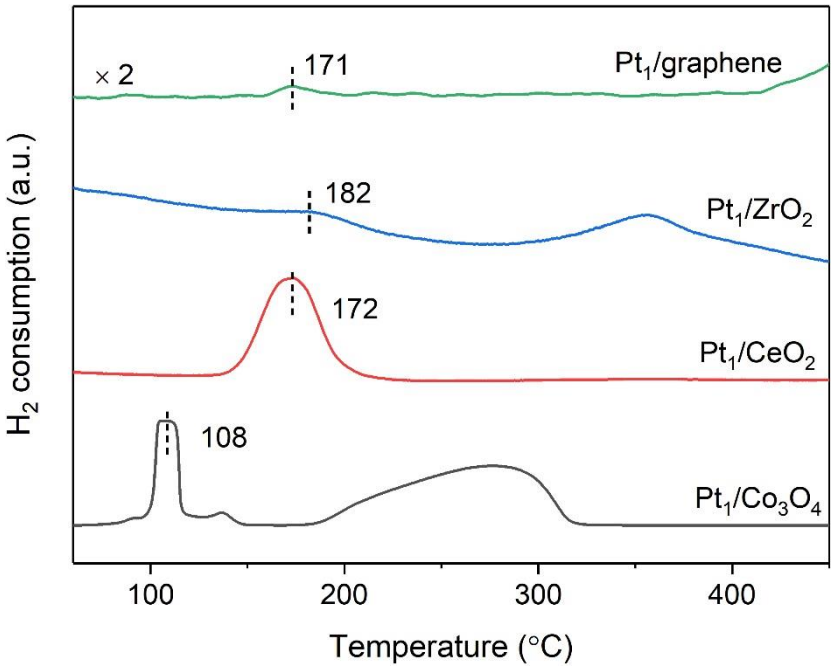

Figure S16. The H_2-TPR profile on Pt_1/Co_3O_4, Pt_1/CeO_2, Pt_1/ZrO_2 and Pt_1/graphene.

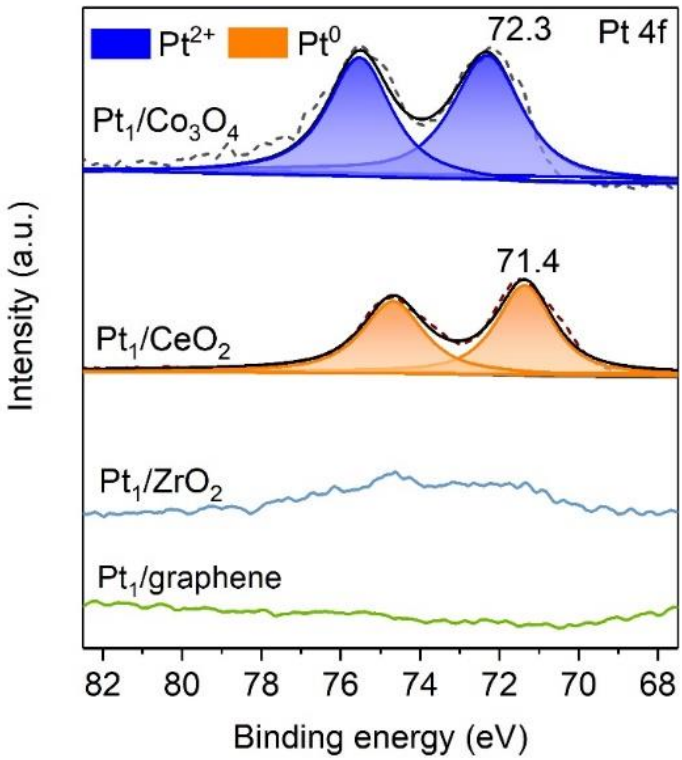

Figure S17. XPS spectra of the used Pt_1/Co_3O_4, Pt_1/CeO_2, Pt_1/ZrO_2, and Pt_1/graphene after 15 cycles of recyclability test in the Pt 4f region.

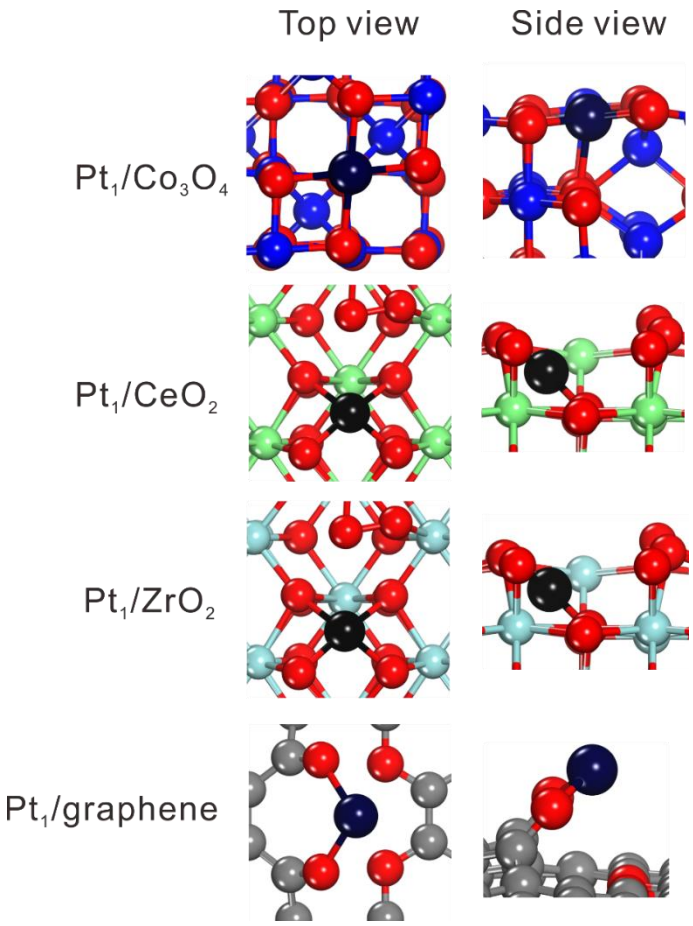

Figure S18. DFT suggested structures for various Pt_1 SACs under reducing conditions. The ball in gray, white, red, green, dark blue, sky blue and black represent carbon, hydrogen, oxygen, cerium, cobalt, zirconium and platinum, respectively.

Note:

Graphene monolayer, Co_3O_4 (100), CeO_2 (110) and ZrO_2 (110) were selected as supports for a single Pt atom with above 16 Å vacuum layer. Pt_1/Graphene was simulated by a (8 × 8) graphene supercell anchoring single Pt atom by two interfacial O in the carbon vacancies as in our previous work[1b]. For Pt_1/Co_3O_4, single Pt atom replaces one of the surface Co atom in a supercell of $(\sqrt{2} \times \sqrt{2})$) nine-atomic-layer Co_3O_4 (100) surface and the bottom three layers are fixed at their bulk positions.[9a] In the structures of Pt_1/CeO_2 and Pt_1/ZrO_2, the CeO_2 (110) and ZrO_2 (110) surfaces were modeled by p (2 × 3) five-atomic-layer supercells with the bottom two layers fixed. The single Pt atom substituted one of the 6-fold Ce or Zr atoms on the surfaces, which leads to the formation of adsorbed surface O_2 species, according to the literature.[10]

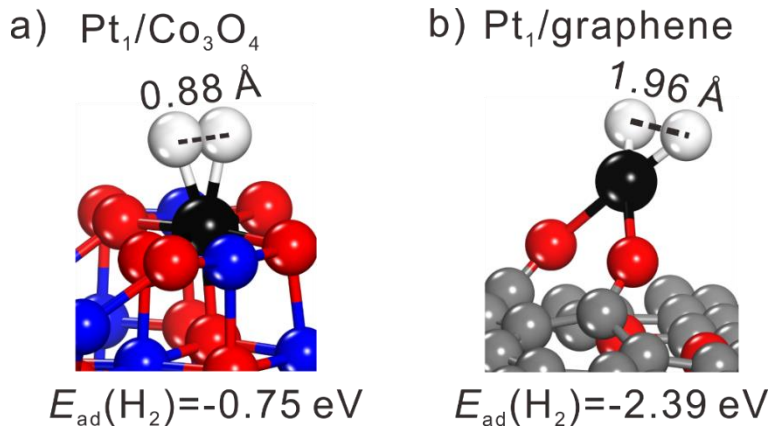

Figure S19. Local configurations for H_2 adsorption on Pt_1/Co_3O_4 (a), Pt_1/graphene (b). The ball in gray, white, red, dark blue and black represent carbon, hydrogen, oxygen, cobalt, and platinum, respectively.

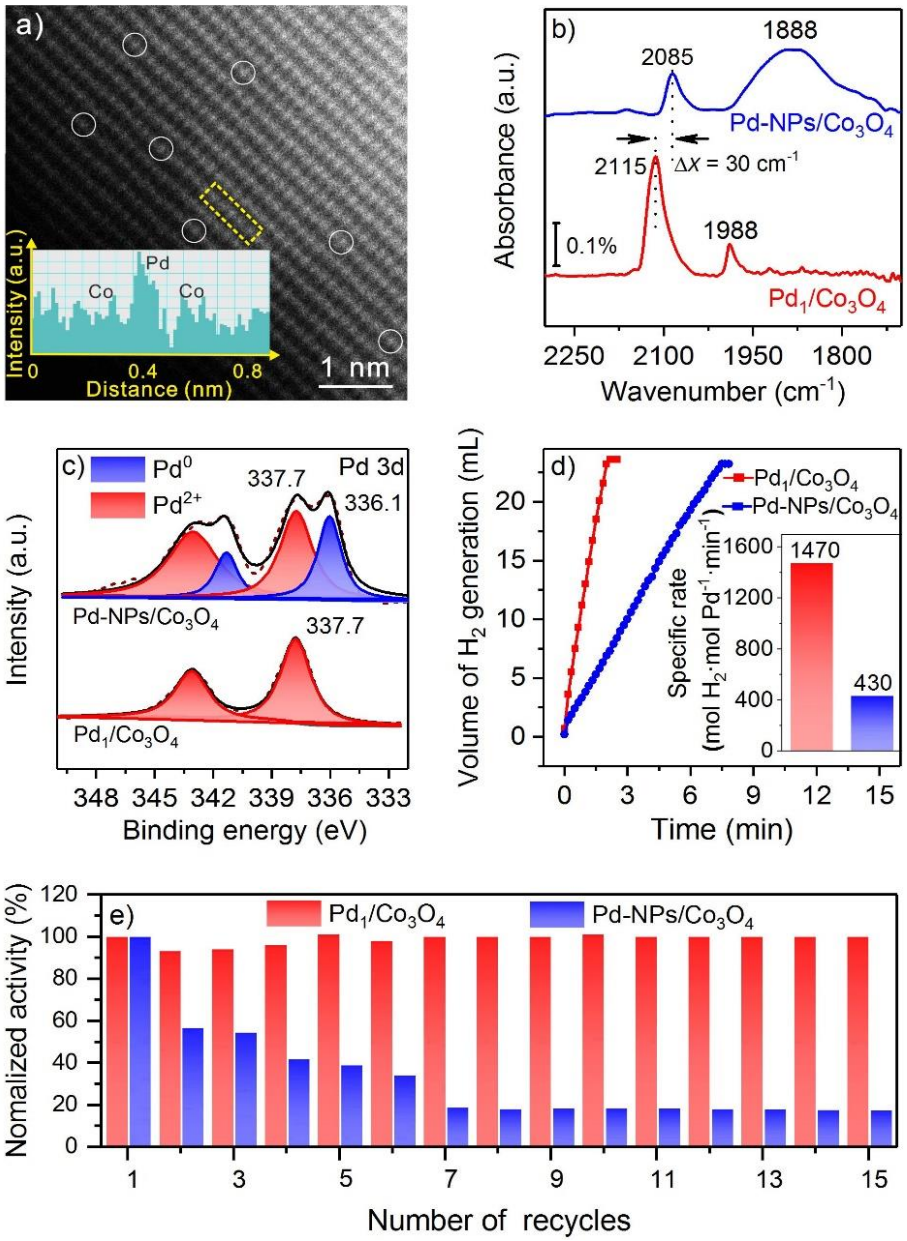

Figure S20. Structural characterization and catalytic performance of Pd_1/Co_3O_4 and Pd-NPs/Co_3O_4 catalysts. (a) A representative HAADF-STEM image of Pd_1/Co_3O_4. (b) DRIFT spectra of CO chemisorption, (c) XPS spectra in the Pd 3d region, (d) plots of hydrogen gas generated as a function of time in the AB dehydrogenation reaction at 25 °C, and (e) recyclability test on Pd_1/Co_3O_4 and Pd-NPs/Co_3O_4. The inset in (a) shows the scanning intensity profile along the yellow dash squire. The inset in (d) shows the corresponding mass specific rates at room temperature.

Notes：

To further examine the remarkable EMSI promotion on both activity and stability of SACs, a Pd_1/Co_3O_4 SAC (Figs. S20a, S21) and a Pd particle sample of Pd-NPs/Co_3O_4 (Fig. S22) were also synthesized. HAADF-STEM confirmed the atomic dispersion of

Pd in Pd_1/Co_3O_4, without any visible NPs/clusters (Figs. S20a, S21). DRIFTS CO chemisorption on Pd-NPs/Co_3O_4 showed two CO peaks at 2085 and 1888 cm^{-1} (Fig. S20b), which are assigned to linear and three-hollow site CO on Pd NPs, respectively.[11] On Pd_1/Co_3O_4, one intense peak at 2115 cm^{-1} and a much weaker one at 1988 cm^{-1}, were observed, which are assigned to linear CO on Pd_1, and probably bridge-bonded CO on ultra-small Pd aggregates, respectively,[11] again supporting that isolated Pd_1 atoms are the dominate form in Pd_1/Co_3O_4. Compared with the peak of linear CO on Pd NPs (2085 cm^{-1}), the large blue shift of 30 cm^{-1} on Pd_1 suggests the Pd_1 atoms are positively charged, along with a greater depletion of 5*d* electronic states.[12] Indeed, XPS showed the valence state of the Pd_1 atoms in Pd_1/Co_3O_4 was close to ~2+ according to the Pd $3d_{5/2}$ peak at 337.7 eV (Fig. S20c), while the Pd-NPs/Co_3O_4 sample showed a mixture of 2+ and zero valence states.

In AB dehydrogenation, the total volume of 23.4 mL of H_2 gas was generated in 2.1 and 7.8 min on Pd_1/Co_3O_4 and Pd-NPs/Co_3O_4, respectively (Fig. S20d). The corresponding mass specific rate for Pd_1/Co_3O_4 was 1470 mol_{H2} mol_{Pd}^{-1} min^{-1}, even higher than Pt_1/Co_3O_4, and about 3.4 times higher than Pd-NPs/Co_3O_4 (430 min^{-1}, the inset of Fig. S20d). Importantly, the Pd_1/Co_3O_4 sample again exhibited excellent recyclability, without any visible activity deactivation and metal sintering/leaching after 15 cycles of recyclability test, in sharp contrast to Pd-NPs/Co_3O_4 (Figs. S20e, S22, S23, and Table S1), again unambiguously supporting the strong EMSI promotion of activity and stability of SACs.

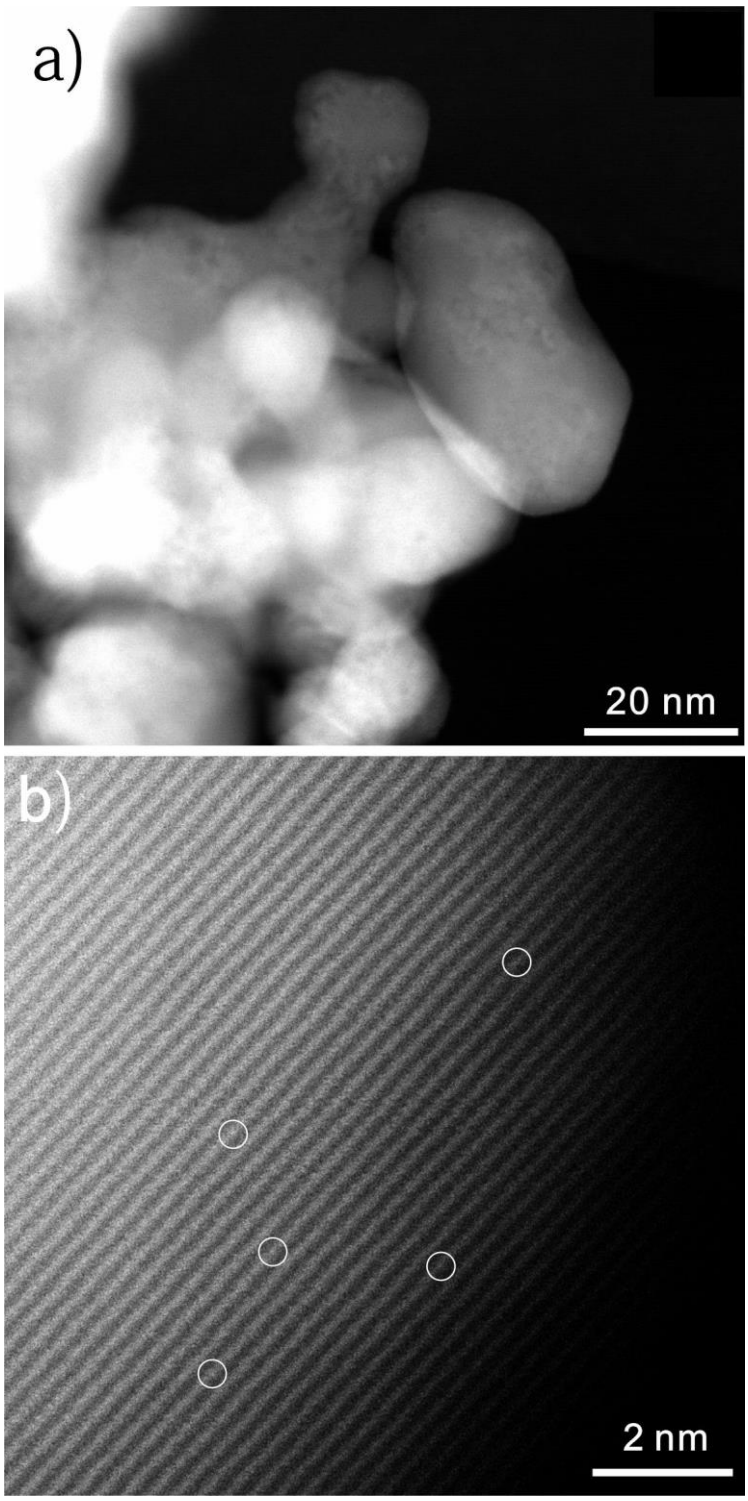

Figure S21. Representative HAADF-STEM images of Pd_1/Co_3O_4 at(a) low- and (b) high-magnifications at other locations. Representive Pd_1 single atoms in (b) are highlighted by the white circles.

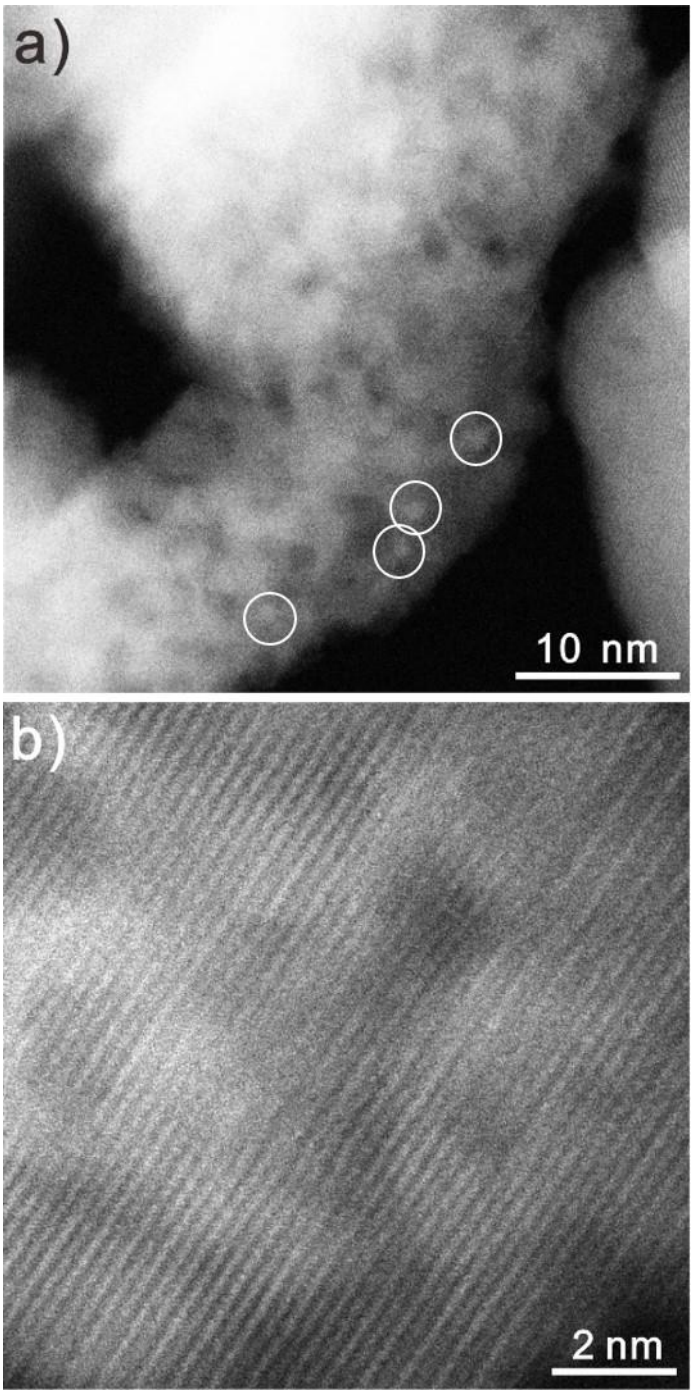

Figure S22. Representative HAADF-STEM images of Pd-NPs/Co_3O_4 at (a) low- and (b) high-magnifications. The white circles highlight the Pd NPs.

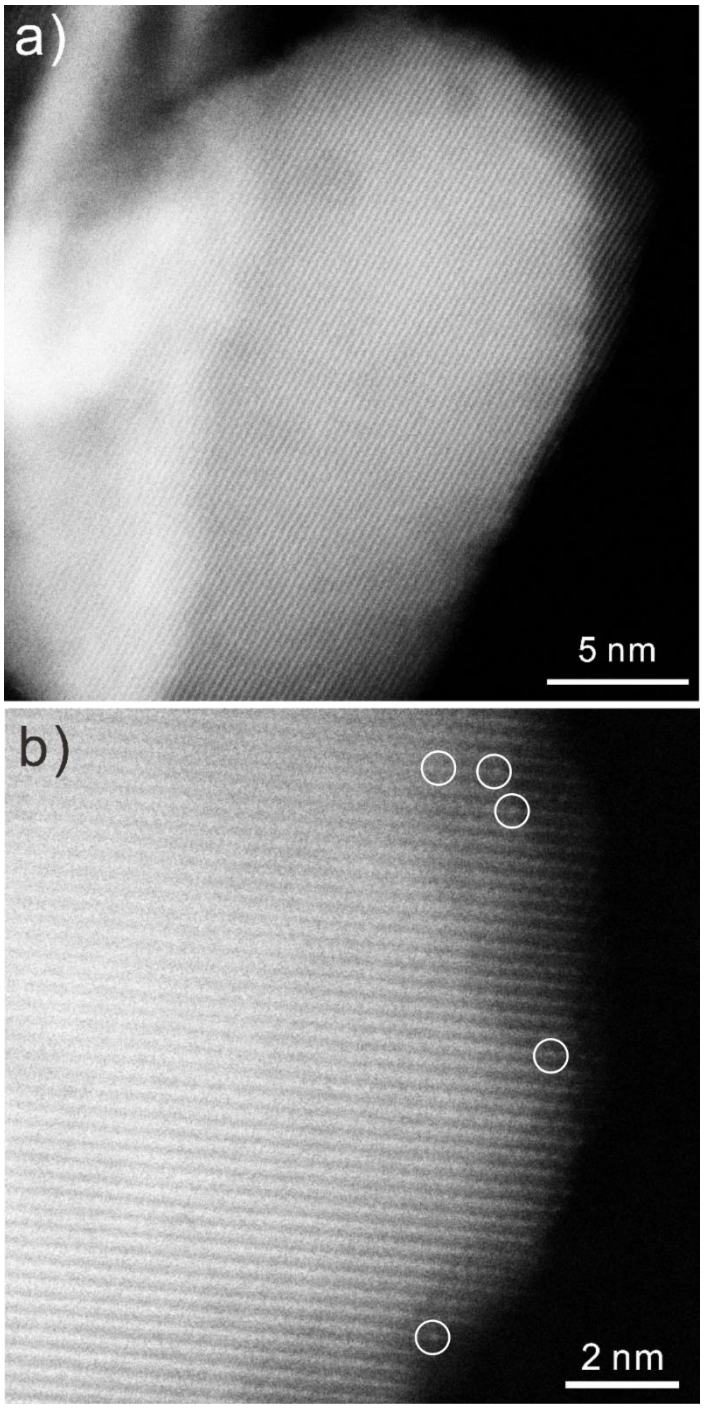

Figure S23. Representative HAADF-STEM images of Pd_1/Co_3O_4 catalyst after 15 cycles of recycling test. No obvious cluster or nanoparticle were observed. Pd_1 atoms in (b) are highlighted by the white circles.

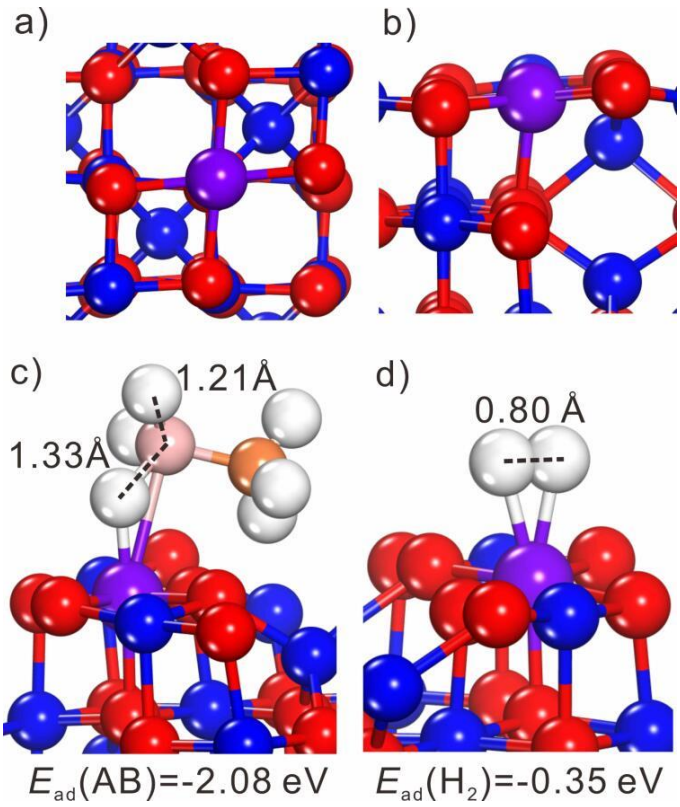

Figure S24. Top (a) and side (b) views of DFT suggested structure for Pd_1/Co_3O_4 SAC. The local configurations for AB (c) and H_2 (d) adsorption on Pd_1/Co_3O_4. The ball in purple, blue, red, pink, orange, and white represent palladium, cobalt, oxygen, boron, nitrogen, and hydrogen, respectively.

Notes:

DFT calculations were further carried out the Pd_1/Co_3O_4. Similar to Pt_1/Co_3O_4, single Pd atom replaces one of the surface Co atom in a supercell of $(\sqrt{2} \times \sqrt{2})$) nine-atomic-layer Co_3O_4 (100) surface (Fig. S24a,b). When AB is absorbed on Pd_1/Co_3O_4, the B-H distance is elongated from 1.21 to 1.33 Å with an adsorption energy of -2.08 eV (Fig. S24c), slightly weaker than on Pt_1/Co_3O_4 (-2.65 eV). H_2 adsorption on Pd_1/Co_3O_4 was very weak about only -0.35 eV (Fig. S24d), which is considerably weaker than H_2 adsorption on Pt_1/Co_3O_4 (-0.75 eV) for accelerating H_2 desorption, explaining the high activity of Pd_1/Co_3O_4.

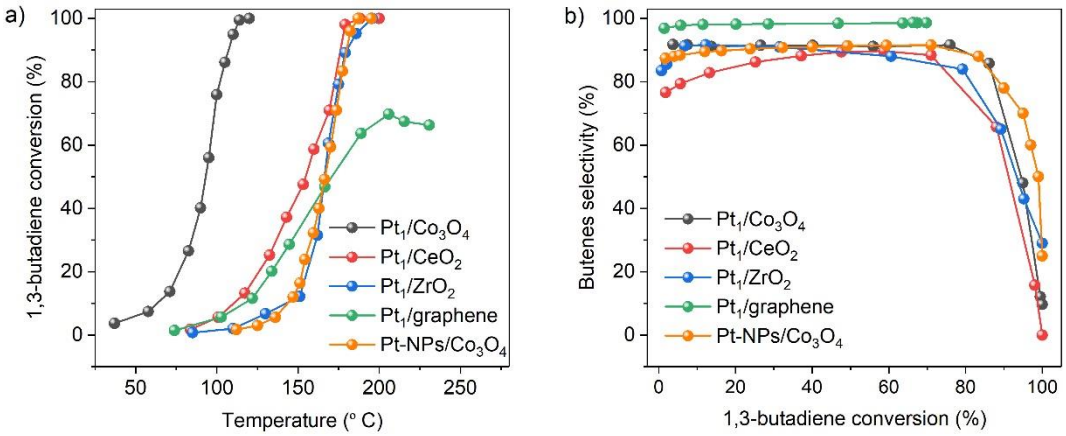

Figure S25. Catalytic performance of Pt_1/Co_3O_4, Pt_1/CeO_2, Pt_1/ZrO_2, and Pt_1/graphene SACs as well as the particle sample of Pt-NPs/Co_3O_4. (a)1,3-butadiene conversion as a function of reaction temperature; (b) The selectivity to butenes as a function of 1,3-butadiene conversion. Reaction conditions: The feed gas was 2.0 % 1,3-butadiene and 4.0 % H_2 with Ar as the balance gas at a total flow rate of 25 mL/min.

Notes:

Selective hydrogenation of 1,3-butadiene to butenes is an important industrial process to purify the alkenes streams from petroleum cracking.[1a] Development of a catalyst with high selectivity to butenes especially 1-butene at near complete conversion of 1,3-butadiene and long durability against deactivation via coking is highly demanded.

Here we further evaluated these four SACs as well as Pt-NPs/Co_3O_4 in selective hydrogenation of 1,3-butadiene. Our preliminary results showed that Pt_1/Co_3O_4 exhibited much higher catalytic activity than other three Pt_1 SACs. The Pt_1/Co_3O_4 achieved 100% conversion at 114 ºC which is much lower than that of Pt_1/CeO_2 (188 ºC) and Pt_1/ZrO_2 (196 ºC). The Pt_1/graphene could only reach 66% conversion even the temperature is 230 ºC (Fig. S25a). Very surprisingly, we found that the hydrogenation activity of Pt_1/Co_3O_4 was even remarkably higher than the nanoparticle sample of Pt-NPs/Co_3O_4. Moreover, the selectivity to butenes over Pt_1/Co_3O_4 was about 92 % at 70 % conversion of 1,3-butadiene, which was also the highest one among these five samples (Fig. S25b).

These new catalytic results further provide strong evidence of the vital role of EMSI in SACs on their catalytic performance of SACs. Apparently, such remarkable EMSI effect on SACs could be general in many catalytic reactions, shedding light on rational design of advanced SACs with high activity.

Table S1. Relative loading of Pt (Pd) loadings on fresh and used samples, as well as the accumulated B content on the used sample, which has a severe impact on catalyst poisoning.

Samples	Pt and Pd loadings (wt %)		Metal loss (%)[b]	B loadings (wt%)
	Fresh samples	Used samples[a]		
Pt_1/Co_3O_4	0.5	0.5	0	1.3
Pt_1/CeO_2	1.1	0.7	36	0.9
Pt_1/ZrO_2	0.2	0.1	50	0.3
Pt_1/graphene	0.4	0.2	50	5.7
Pt-NPs/Co_3O_4	13.5	9.4	30	7.9
Pd_1/Co_3O_4	0.3	0.3	0	2.2
Pd-NPs/Co_3O_4	0.7	0.3	57	2.3

[a]the metal loadings of the used samples after 15 cycles of recycling test.

[b]the metal loss was calculated by the equation:

$$\text{Metal loss} = (M_{Fresh} - M_{Used}) / M_{Fresh} \times 100\%,$$

where M_{Fresh} is the metal loadings of the fresh samples, M_{Used} is the metal loadings of the fresh samples

Table S2 Structural parameters of the Pt_1 SACs and the Pt foil and PtO_2 references extracted from quantitative EXAFS curve-fittings using the ARTEMIS module of IFEFFIT.

Sample	Path	CNs	*R*(Å)	σ^2 ($10^{-3}Å^2$)	ΔE_0 (eV)	*R*-factor
Pt foil	Pt-Pt	12	2.77			
PtO_2	Pt-O	6.0	2.07			
	Pt-Pt	6.0	3.10			
Pt_1/Co_3O_4	Pt-O	5.7	2.00	2.5	9.5	0.001
	Pt-Co	4.8	2.91	9.3	0.1	
Pt_1/CeO_2	Pt-O	4.9	2.00	3.0	10.0	0.006
Pt_1/ZrO_2	Pt-O	4.8	1.99	2.9	8.9	0.003
Pt_1/graphene	Pt-O1	2.0	1.96	6.7	9.9	0.007
	Pt-O2	2.0	2.05	6.7	9.9	

CNs, coordination numbers; R, bonding distance; σ^2, Debye-Waller factor; ΔE_0, inner potential shift.

Table S3. A comparison of catalytic activities over various metal catalysts in hydrolysis of AB measured in this work and the ones reported in literature.

Catalyst	T (°C)	Specific rate ($mol \cdot H_2 \cdot molmetal^{-1} \cdot min^{-1}$)	Ea ($kJ \cdot mol^{-1}$)	Reference
Pt_1/Co_3O_4	25	1220	37.4	This work
Pd_1/Co_3O_4	25	1470	55.4	This work
Pt_1/CeO_2	25	18	78.2	This work
Pt_1/ZrO_2	25	65	80.6	This work
Pt_1/graphene	25	160	69.8	This work
Pt-NPs/Co_3O_4	25	349	-	This work
Pt/Carbon	25	310	-	This work
Pt/SiO_2	25	180	-	This work
Pt/Al_2O_3	25	180	-	This work
Pd-NPs/Co_3O_4	25	430	-	This work
PEI-GO/$Pt_{0.17}Co_{0.8}$	25	378	51.6	Ref[13]
$Co_{0.32}$@$Pt_{0.68}$/C	25	248.5	41.5	Ref[14]
Pt/CeO_2/RGO	25	48	-	Ref[15]
Pt/γ Al_2O_3	25	222	39	Ref[16]
Pt-MIL-101	25	260	40.7	Ref[17]
Pd@Co/grapheme	25	409	-	Ref[18]
$Co_{35}Pd_{65}$/C annealed	25	54.9	27.5	Ref[19]
Pd/zeolite	25	6.25	56	Ref[20]
PSSA-co-MA-Pd	25	20	44	Ref[21]
Pd/γ Al_2O_3	25	1.39	-	Ref[22]
Ru@Co/grapheme	25	344	-	Ref[23]
RuCo/γ Al_2O_3	25	33	47	Ref[24]
Ru@Co/C	25	320	21.16	Ref[25]
RuCo/$Ti_3C_2X_2$	25	896	31.1	Ref[26]

Table S4 Structural parameters of the optimized Pt_1 SACs under the reducing conditions by DFT calculations.

Sample	DFT		
	Path	**CNs**	***R*(Å)**
Pt_1/Co_3O_4	Pt-O1	1	1.99
	Pt-O2	3	2.02
	Pt-O3	1	2.03
	Pt-Co1	1	2.92
	Pt-Co2	2	2.94
	Pt-Co3	1	2.96
Pt_1/CeO_2	Pt-O1	2	2.00
	Pt-O2	2	2.02
Pt_1/ZrO_2	Pt-O1	2	2.01
	Pt-O2	1	2.02
	Pt-O3	1	2.03
Pt_1/graphene*	Pt-O	2	1.96

*Notes: AB is known as an excellent reducing agent. The terminal dioxygen of Pt_1/graphene as suggested by XAFS and DFT calculations in our previous work is likely stripped off during the reaction[1b], which gives a Pt-O coordination number of 2.

Table S5. Calculated binding energies of Pt_1 atom in the samples of Pt_1/Co_3O_4, Pt_1/CeO_2, Pt_1/ZrO_2, and Pt_1/graphene.

Samples	Binding energy (eV)
Pt_1/Co_3O_4	-8.43
Pt_1/CeO_2	-8.34
Pt_1/ZrO_2	-7.23
Pt_1/graphene	-2.31

References

(1) (a) Yan, H.; Cheng, H.; Yi, H.; Lin, Y.; Yao, T.; Wang, C. L.; Li, J. J.; Wei, S. Q.; Lu, J. L., Single-atom Pd_1/graphene catalyst achieved by atomic layer deposition: Remarkable performance in selective hydrogenation of 1,3-butadiene. *J. Am. Chem. Soc.* **2015,** *137*, 10484-10487. (b) Yan, H.; Lin, Y.; Wu, H.; Zhang, W. H.; Sun, Z. H.; Cheng, H.; Liu, W.; Wang, C. L.; Li, J. J.; Huang, X. H.; Yao, T.; Yang, J. L.; Wei, S. Q.; Lu, J. L., Bottom-up precise synthesis of stable platinum dimers on graphene. *Nat. Commun.* **2017,** *8*, 1070.

(2) (a) Sun, C.; Li, H.; Zhang, H.; Wang, Z.; Chen, L., Controlled synthesis of CeO_2 nanorods by a solvothermal method. *Nanotechnology* **2005,** *16*, 1454. (b) Mai, H.-X.; Sun, L.-D.; Zhang, Y.-W.; Si, R.; Feng, W.; Zhang, H.-P.; Liu, H.-C.; Yan, C.-H., Shape-selective synthesis and oxygen storage behavior of ceria nanopolyhedra, nanorods, and nanocubes. *J. Phys. Chem. B* **2005,** *109*, 24380-24385. (c) Pan, C.; Zhang, D.; Shi, L.; Fang, J., Template-free synthesis, controlled conversion, and CO oxidation properties of CeO_2 nanorods, nanotubes, nanowires, and nanocubes. *Eur. J. Inorg. Chem.* **2008,** *2008*, 2429-2436.

(3) Lu, J.; Fu, B.; Kung, M. C.; Xiao, G.; Elam, J. W.; Kung, H. H.; Stair, P. C., Coking- and sintering-resistant palladium catalysts achieved through atomic layer deposition. *Science* **2012,** *335*, 1205-1208.

(4) Lu, J.; Stair, P. C., Nano/subnanometer Pd nanoparticles on oxide supports synthesized by AB-type and low-temperature ABC-type atomic layer deposition: Growth and morphology. *Langmuir* **2010,** *26*, 16486-16495.

(5) (a) Yadav, M.; Xu, Q., Liquid-phase chemical hydrogen storage materials. *Energ Environ Sci* **2012,** *5*, 9698-9725. (b) Qiao, B.; Wang, A.; Yang, X.; Allard, L. F.; Jiang, Z.; Cui, Y.; Liu, J.; Li, J.; Zhang, T., Single-atom catalysis of CO oxidation using Pt_1/FeO_x. *Nat. Chem.* **2011,** *3*, 634-41.

(6) (a) Kresse, G.; Furthmuller, J., Efficiency of ab-initio total energy calculations for metals and semiconductors using a plane-wave basis set. *Comp. Mater. Sci.* **1996,** *6*, 15-50. (b) Kresse, G.; Furthmuller, J., Efficient iterative schemes for ab initio total-energy calculations using a plane-wave basis set. *Phys. Rev. B* **1996,** *54*, 11169-11186.

(7) Perdew, J. P.; Burke, K.; Ernzerhof, M., Generalized gradient approximation made simple. *Phys. Rev. Lett.* **1996,** *77*, 3865-3868.

(8) Dudarev, S. L.; Botton, G. A.; Savrasov, S. Y.; Humphreys, C. J.; Sutton, A. P., Electron-energy-loss spectra and the structural stability of nickel oxide: An LSDA+U study. *Phys. Rev. B* **1998,** *57*, 1505-1509.

(9) (a) Gao, S.; Sun, Z. T.; Liu, W.; Jiao, X. C.; Zu, X. L.; Hu, Q. T.; Sun, Y. F.; Yao, T.; Zhang, W. H.; Wei, S. Q.; Xie, Y., Atomic layer confined vacancies for atomic-level insights into carbon dioxide electroreduction. *Nat. Commun.* **2017,** *8*, 14503. (b) Wang, C. L.; Gu, X. K.; Yan, H.; Lin, Y.; Li, J. J.; Liu, D. D.; Li, W. X.; Lu, J. L., Water-mediated Mars-van Krevelen mechanism for CO oxidation on ceria-supported single-atom Pt_1 catalyst. *ACS Catal.* **2017,** *7*, 887-891. (c) Chen, H. Y. T.; Tosoni, S.; Pacchioni, G., Adsorption of ruthenium atoms and clusters on anatase TiO_2 and tetragonal ZrO_2(101) surfaces: A comparative DFT study. *J. Phys. Chem. C* **2015,** *119*, 10856-10868.

(10) Tang, Y.; Wang, Y.-G.; Li, J., Theoretical investigations of $Pt_1@CeO_2$ single-atom catalyst for CO oxidation. *J. Phys. Chem. C* **2017,** *121*, 11281-11289.

(11) Lear, T.; Marshall, R.; Antonio Lopez-Sanchez, J.; Jackson, S. D.; Klapötke, T. M.; Bäumer, M.; Rupprechter, G.; Freund, H.-J.; Lennon, D., The application of infrared spectroscopy to probe the surface morphology of alumina-supported palladium catalysts. *J. Chem. Phys.* **2005,** *123*, 174706.

(12) (a) Rodriguez, J. A.; Kuhn, M., Chemical and electronic properties of Pt in bimetallic surfaces: Photoemission and CO-chemisorption studies for Zn/Pt(111). *J. Chem. Phys.* **1995,** *102*, 4279-4289. (b) Davidson, E. R.; Kunze, K. L.; Machado, F. B.; Chakravorty, S. J., The transition metal-carbonyl bond. *Acc. Chem. Res.* **1993,** *26*, 628-635.

(13) Li, M.; Hu, J.; Chen, Z.; Lu, H., A high-performance Pt–Co bimetallic catalyst with polyethyleneimine decorated graphene oxide as support for hydrolysis of ammonia borane. *RSC Adv.* **2014,** *4*, 41152-41158.

(14) Yang, X.; Cheng, F.; Tao, Z.; Chen, J., Hydrolytic dehydrogenation of ammonia borane catalyzed by carbon supported Co core–Pt shell nanoparticles. *J. Power Sources* **2011,** *196*, 2785-2789.

(15) Wang, X.; Liu, D. P.; Song, S. Y.; Zhang, H. J., Graphene oxide induced formation of Pt-CeO_2 hybrid nanoflowers with tunable CeO_2 thickness for catalytic hydrolysis of ammonia borane. *Chem.-Eur. J.* **2013,** *19*, 8082-8086.

(16) Chandra, M.; Xu, Q., Room temperature hydrogen generation from aqueous ammonia-borane using noble metal nano-clusters as highly active catalysts. *J. Power Sources* **2007,** *168*, 135-142.

(17) Aijaz, A.; Karkamkar, A.; Choi, Y. J.; Tsumori, N.; Ronnebro, E.; Autrey, T.; Shioyama, H.; Xu, Q., Immobilizing highly catalytically active Pt nanoparticles inside the pores of metal-organic framework: A double solvents approach. *J. Am. Chem. Soc.* **2012,** *134*, 13926-9.

(18) Wang, J.; Qin, Y.-L.; Liu, X.; Zhang, X.-B., In situ synthesis of magnetically recyclable graphene-supported Pd@Co core–shell nanoparticles as efficient catalysts for hydrolytic dehydrogenation of ammonia borane. *J. Mater. Chem.* **2012,** *22*, 12468.

(19) Sun, D. H.; Mazumder, V.; Metin, O.; Sun, S. H., Catalytic hydrolysis of ammonia borane via cobalt palladium nanoparticles. *ACS Nano* **2011,** *5*, 6458-6464.

(20) Rakap, M.; Özkar, S., Zeolite confined palladium(0) nanoclusters as effective and reusable catalyst for hydrogen generation from the hydrolysis of ammonia-borane. *Int. J. Hydrogen Energy* **2010,** *35*, 1305-1312.

(21) Metin, Ö.; Şahin, Ş.; Özkar, S., Water-soluble poly(4-styrenesulfonic acid-co-maleic acid) stabilized ruthenium(0) and palladium(0) nanoclusters as highly active catalysts in hydrogen generation from the hydrolysis of ammonia–borane. *Int. J. Hydrogen Energy* **2009,** *34*, 6304-6313.

(22) Xu, Q.; Chandra, M., A portable hydrogen generation system: Catalytic hydrolysis of ammonia–borane. *J. Alloys Compd.* **2007,** *446*, 729-732.

(23) Cao, N.; Su, J.; Luo, W.; Cheng, G., Graphene supported Ru@Co core–shell nanoparticles as efficient catalysts for hydrogen generation from hydrolysis of ammonia borane and methylamine borane. *Catal. Commun.* **2014,** *43*, 47-51.

(24) Rachiero, G. P.; Demirci, U. B.; Miele, P., Bimetallic RuCo and RuCu catalysts supported on γ-Al_2O_3. A comparative study of their activity in hydrolysis of ammonia-borane. *Int. J. Hydrogen Energy* **2011,** *36*, 7051-7065.

(25) Cao, N.; Su, J.; Hong, X. L.; Luo, W.; Cheng, G. Z., In situ facile synthesis of ru-based core-shell nanoparticles supported on carbon black and their high catalytic activity in the dehydrogenation of amine-boranes. *Chem. Asian J.* **2014,** *9*, 562-571.

(26) Li, X.; Zeng, C.; Fan, G., Magnetic RuCo nanoparticles supported on two-dimensional titanium carbide as highly active catalysts for the hydrolysis of ammonia borane. *Int. J. Hydrogen Energy* **2015,** *40*, 9217-9224.